JSACE 2/40

Modelling of the Nonlinear Behaviour of the Steel and GFRP Reinforced Recycled Aggregate Concrete Slabs Using ANSYS

Received 2026/01/29

Accepted after revision 2026/04/21

Modelling of the Nonlinear Behaviour of the Steel and GFRP Reinforced Recycled Aggregate Concrete Slabs Using ANSYS

Irina Kerelezova*

University of Architecture, Civil Engineering and Geodesy, Faculty of Civil Engineering, 1 Hr. Smirnenski Blvd. Sofia 1046, Bulgaria, igk_fce@uacg.bg

*Corresponding author: **igk_fce@uacg.bg**

https://doi.org/10.5755/j01.sace.44189

Abstract

The use of recycled aggregates in structural reinforced concrete remains limited because of concerns about material quality and the ability to predict structural behaviour reliably. An even greater challenge is the replacement of conventional steel reinforcement with composite reinforcement. Numerical modelling provides an opportunity to improve predictions and support the design of concrete incorporating recycled aggregates. This study investigates two approaches to modelling reinforcement bars (discrete and smeared) in one-way reinforced slabs subjected to three-point bending using the SOLID 65 finite element in ANSYS. Four slabs are modelled using two types of concrete (ordinary concrete and RAC) and two types of reinforcement (steel and GFRP). The models are verified against experimental results. The ability of the two modelling approaches to capture cracking loads and load-deflection behaviour for different combinations of concrete and reinforcement materials is demonstrated.

Keywords: ANSYS software; glass fiber reinforced polymers (GFRP); nonlinear finite element modelling; recycled aggregate concrete (RAC); SOLID 65.

Introduction

Recycled aggregate concrete (RAC) offers opportunities to improve resource efficiency in construction (Pacheco et al., 2023; Vintimilla & Etxeberria, 2023). However, steel reinforcement in RAC structures is considered more vulnerable to corrosion in aggressive environments than in conventional natural aggregate concrete (NAC). Replacing steel rebars with composite reinforcement such as GFRP can help address durability issues associated with RAC, including accelerated carbonation and increased chloride permeability (Pacheco et al., 2023; Vintimilla & Etxeberria, 2023). In addition, GFRP reinforcement is an attractive alternative to steel because of its lower density, higher tensile strength, and much lower thermal conductivity.

The present study forms part of broader research on improving RAC. The effects of concrete mix design on the strength and elastic modulus of RAC, the bond between RAC and GFRP rebars, and other characteristics were investigated by Zaharieva et al. (2022). In that study, the authors compared the experimental results with values calculated according to the CEB-FIP Model Code 1990 (CEB-FIP, 1993). Subsequent work showed that the characteristics of RAC containing 30% recycled aggregate are very similar to those of natural aggregate concrete (Zaharieva et al., 2022; Traykova et al., 2024).

ktu 1922

Journal of Sustainable Architecture and Civil Engineering
Vol. 2 / No. 40 / 2026
pp. 56-71
DOI 10.5755/J01.SACE.44189

Using high-tech construction materials such as GFRP as reinforcement in RAC structural elements presents challenges for modelling slab reinforcement. To validate the proposed finite element approach, numerical results are compared with experimental results obtained from four slab specimens. There are several ways to represent reinforcement in reinforced concrete models. The most common approach is to add link (bar) finite elements connected to the nodes of solid or shell elements. In some software, reinforcement can be incorporated directly into the finite elements (e.g., SOLID 65 in ANSYS), allowing it to be represented more directly. Even in this case, however, many authors use link elements to model reinforcement bars. Based on the capabilities of the SOLID 65 finite element (FE) in ANSYS, this study compares two reinforcement modelling approaches: discrete and smeared reinforcement.

Scope and Challenges of the Study

The main challenge is how to model reinforcement in elements subjected to bending, such as beams and slabs. ANSYS provides the SOLID 65 finite element for modelling reinforced concrete. This three-dimensional, eight-node element allows reinforcement to be incorporated in three different directions. The reinforcement amount is defined by its ratio to the element volume (ANSYS, 2024). The element can simulate concrete crushing and crack development. Given these capabilities, SOLID 65 is well suited to modelling reinforced-concrete structures. Nevertheless, most authors use a combination of finite elements. For reinforced-concrete beams, reinforcement is often modelled with LINK 181 (or the older LINK 8), a bar element (Tjtradi et al., 2017; Manjunath & Prabhakara, 2019; Musmar et al., 2014; Jebur, 2021; Smarzewski & Słowik, 2023; Bondok et al., 2023). These bar elements are connected to the nodes of SOLID 65 elements, which are then used only to represent the concrete. Only a few researchers have used SOLID 65 to model both concrete and reinforcement. Parvanova et al. (2005) and Dahmani et al. (2010) represented reinforcement as distributed within the lower layer of a beam using the full capabilities of SOLID 65. Dere and Dede (2011) developed a discrete reinforcement model by placing the reinforcement at its actual position within the cross-section of a reinforced-concrete frame.

For slabs, modelling individual reinforcement bars is more difficult, yet some researchers still use LINK elements to represent reinforcement (Tran & Cajka, 2022; Assad et al., 2022; Emarah, 2019; Kaya & Anil, 2021; Mahmoud et al., 2024). Tran and Cajka (2022) investigated fibre-reinforced concrete and the influence of several material parameters, which may explain their use of LINK elements for reinforcement. Assad et al. (2022) and Emarah (2019) studied reinforced slabs with different FRP strengthening configurations but also used LINK elements for reinforcement. Kaya and Anil (2021) investigated a reinforced slab, whereas Mahmoud et al. (2024) investigated a steel-reinforced concrete hidden and wide beam; both studies likewise used LINK elements to model the reinforcement bars. Only a few researchers, such as Gherbi et al. (2018) and Avci and Bhargava (2019), have used the full capabilities of SOLID 65. Gherbi et al. (2018) noted that LINK-element modelling is more suitable for simple structures such as beams and less appropriate for slabs. They used a smeared reinforcement approach, representing reinforcement as a layer with an average reinforcement ratio at the bottom of the slab. Avci and Bhargava (2019) adopted a similar uniformly distributed reinforcement approach. Overall, relatively few studies exploit the full potential of SOLID 65 for reinforcement modelling, and discrete modelling is particularly uncommon.

In the authors' view, the most suitable way to model slab reinforcement is to use the capabilities of SOLID 65. The main objective of this study is therefore to compare two reinforcement modelling approaches - discrete and smeared - using SOLID 65. Within this element, the reinforcement bar and its direction are assigned at the centre of the finite element. In the discrete approach, the reinforcement is placed at its actual position, whereas in the smeared approach an average reinforcement ratio is assigned to the bottom layer of the slab.

Materials and Methods

Experimental Data for the Slabs

In this study, experimental results from four one-way reinforced slabs subjected to bending are used. Two slabs are made of NAC and reinforced with either steel or GFRP rebars, designated "NAC-Steel" and "NAC-GFRP", respectively. The other two slabs are made of RAC30 and use two GFRP reinforcement arrangements, designated "RAC-GFRP1" and "RAC-GFRP2". The static scheme and reinforcement distribution are shown in **Fig. 1** (Zaharieva et al., 2022; Traykova et al., 2024). Reinforcement material data are presented in **Table 1**, and data for NAC and RAC30 are presented in **Table 2**.

Fig. 1

Reinforced slabs: **a** and **b** reinforcement distribution; **c** static scheme.

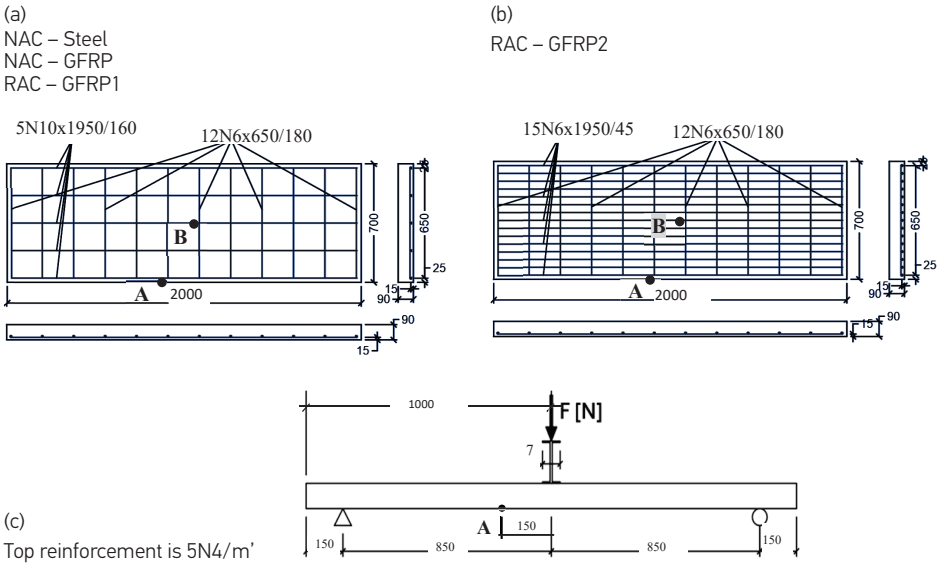


Table 1

Reinforcement material data (Zaharieva et al., 2022; Traykova et al., 2024).

Characteristics	Unit	Steel	GFRP
Density	kg/m^3	7850	1850
Young's modulus	N/mm^2	200 000	46 000

Table 2

Concrete material data (Zaharieva et al., 2022).

Characteristics	Unit	NAC	RAC30
Density	kg/m^3	2390	2310
f_c at 28 days	N/mm^2	52	51
f_t at 28 days	N/mm^2	3.3	3.2
Young's modulus	N/mm^2	35 400	35 600

The experimental programme was conducted at the University of Architecture, Civil Engineering and Geodesy, Sofia, Bulgaria, as part of the project "Clean Technologies for Sustainable Environment - Water, Waste, Energy for Circular Economy" (Clean&Circle). A detailed analysis of the experimental results was published by Zaharieva et al. (2022) and Traykova et al. (2024). Both concrete types (NAC and RAC) are modelled in ANSYS using SOLID 65 material properties.

Modelling Options

SOLID 65 uses a smeared-crack approach to model cracking in tensile zones and a plasticity algorithm to account for concrete crushing in compression. A nonlinear material law is used to

represent the nonlinear response of quasi-brittle materials. It is based on the Willam-Warnke constitutive model for the triaxial behaviour of concrete (ANSYS, 2024).

The failure criterion requires five strength parameters to define the failure surface: f_t, f_c, f_{cb}, f_1 and f_2. However, the criterion can be specified using only two constants f_t and f_c which serve as the basis for defining the other three constants. The default correlations implemented in ANSYS and used in this study are $f_{cb}=1.2f_c$; $f_1=1.45f_c$; $f_2=1.725f_c$ for $|\sigma_h^a|\leq\sqrt{3}\ f_c$ (ANSYS, 2024).

To apply the Willam-Warnke theoretical model and the full capabilities of SOLID 65 to the present problem, several assumptions and preliminary simulations are made.

The experimental data contain no information on biaxial or hydrostatic stress states. Therefore, the default correlations implemented in the software are used in this study.

Two types of concrete are considered in this study. The first is natural aggregate concrete (NAC), and the second is RAC30, which has strength characteristics very similar to those of NAC (Table 2). Therefore, both materials can be represented using the Willam-Warnke theoretical model.

All KEYOPT settings for the elements are left at their default values. SOLID 65 does not provide an option to model dowel action; therefore, this effect cannot be taken into account. A perfect bond between the reinforcement and concrete is assumed. This is a significant limitation of the present study, particularly for GFRP reinforcement.

Because SOLID 65 uses smeared-crack theory, stresses are monitored at each Gauss point, allowing cracks to open in three mutually perpendicular directions. Concrete crushing is also included in SOLID 65. Consequently, 16 Gauss-point status combinations are possible across the three directions, including crack opening, crack closing, crushing, or none of these states.

Shear transfer across a crack is represented in SOLID 65 by two coefficients, β1 for an open crack and β2 for a closed crack. These shear-retention factors range from 0 (no aggregate interlock) to 1 (full aggregate interlock). Their values affect numerical convergence. In this study, the influence of these parameters on convergence is examined. The results show that setting both β1 and β2 to zero prevents convergence. When β1 = 0 and β2 is varied, the solution does not reach the final stage. When both coefficients are non-zero, the solution converges and the resulting load-deflection curves are practically identical. Similar conclusions were reported by Smarzewski and Słowik (2023), Parvanova et al. (2005), and Dere and Dede (2011), who recommended values between 0.6 and 1.0 for β1 and β2, respectively. For all solutions presented in the following section, β1 = 0.6 and β2 = 1.0 are used for both natural aggregate concrete and recycled aggregate concrete.

Regarding post-cracking modelling, SOLID 65 offers options with or without stress relaxation. When stress relaxation is included, the reduction in maximum stress can be represented using a multiplier. According to the ANSYS manual, stress relaxation is used only to accelerate convergence (ANSYS, 2024). For each slab, analyses were performed to assess the influence of this option. No effect on convergence or the load-deflection curves was observed; therefore, stress relaxation was excluded from the solutions presented in the following section.

Reinforcement can be modelled as an elastic-plastic material. At the beginning of the study, such a model was used for the NAC-Steel slab. This resulted in yielding of the reinforcement at a deflection of approximately 11-12 mm. No yielding was reported in the experiment. This discrepancy is probably due to the numerical models being stiffer than the experimental specimen. To avoid introducing a disagreement that would require more detailed investigation, the analyses presented in the following section assume linear-elastic behaviour of the steel, consistent with the experimental observations.

GFRP is a brittle material with very high tensile strength. The experimental data do not indicate that the tensile strength was reached; therefore, the GFRP reinforcement is also modelled as linear elastic.

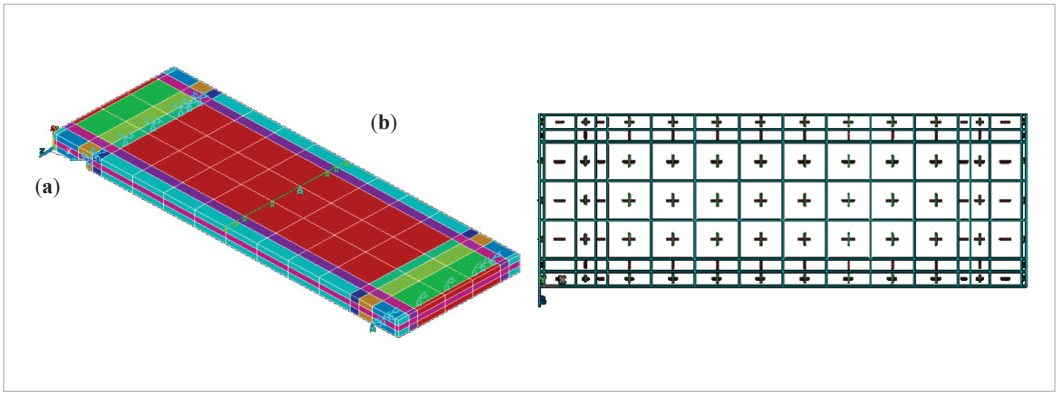
Numerical Modelling

To investigate reinforcement modelling, two model types were developed. Both models were used for three slabs (NAC-Steel, NAC-GFRP, and RAC-GFRP1), whereas only one model was used for the fourth slab, RAC-GFRP2 (Fig. 1). Model 1 represents discrete reinforcement, while Model 2 represents smeared reinforcement. In both models, supports are defined by restraining all degrees of freedom of the nodes along one line on the left and selected degrees of freedom along one line on the right, allowing axial movement in the X direction. Loading is applied through displacement control at the midspan line of nodes, which are coupled in the Y direction.

- **Model 1** is constructed so that each reinforcement bar is placed at its actual position in the slab (see Fig. 1(a)). According to the SOLID 65 formulation, the reinforcement passes through the centre of the element. The finite-element mesh is therefore generated so that element sizes and positions follow the reinforcement layout. The FE mesh and reinforcement-bar positions are shown in Fig. 2.

Fig. 2

FE mesh: **a** real constants shown by colour; **b** reinforcement-bar positions and directions.



This approach requires 14 different real constants (shown by colours in Fig. 2) to account for the different finite-element dimensions and rebars in the bottom reinforcement. Details of the finite-element sizes and real constants for the bottom layer of the slab are presented in Table 3. The middle layer uses a plain-concrete real constant. Another 14 real constants are calculated in a similar manner for the top layer.

Table 3

SOLID 65 real constants for Model 1.

Real constant	Element sizes [mm]	Reinforcement in direction X	Reinforcement in direction Y	Volume [mm3]		
1	20/60/30	1N10	1N6	36 000	0.04361	0.04717
2	20/50/30	–	1N6	30 000	–	0.04717
3	20/160/30	1N10	1N6	96 000	0.01635	0.004717
4	130/60/30	1N10	–	234 000	0.04361	–
5	130/50; 50/50	–	–	–	–	–
6	130/160/30	1N10	–	624 000	0.01635	–
7	80/60/30	1N10	1N6	144 000	0.04361	0.01179
8	80/50/30	–	1N6	120 000	–	0.01179
9	80/160/30	1N10	1N6	384 000	0.01636	0.01179
10	50/60/30	1N10	–	90 000	0.04361	–
11	50/160/30	1N10	–	240 000	0.01636	–
12	180/60/30	1N10	1N6	324 000	0.04361	0.005241
13	180/50/30 (	–	1N6	270 000	–	0.00524
14	180/160/30	1N10	1N6	864 000	0.01635	0.005241

Model 2 uses the smeared-reinforcement approach, the simplest variant of reinforcement modelling. A regular mesh is used, and reinforcement is represented as distributed reinforcement with an average ratio in the two directions. Only three real constants are required, one for each layer. The finite-element mesh and real constants (shown by colours) are presented in Fig. 3. Table 4 gives the reinforcement direction, quantity, and corresponding real constants for the different slabs. For Model 2, the mesh is relatively dense, with an element size of 75/70/30 mm and an aspect ratio close to 1.

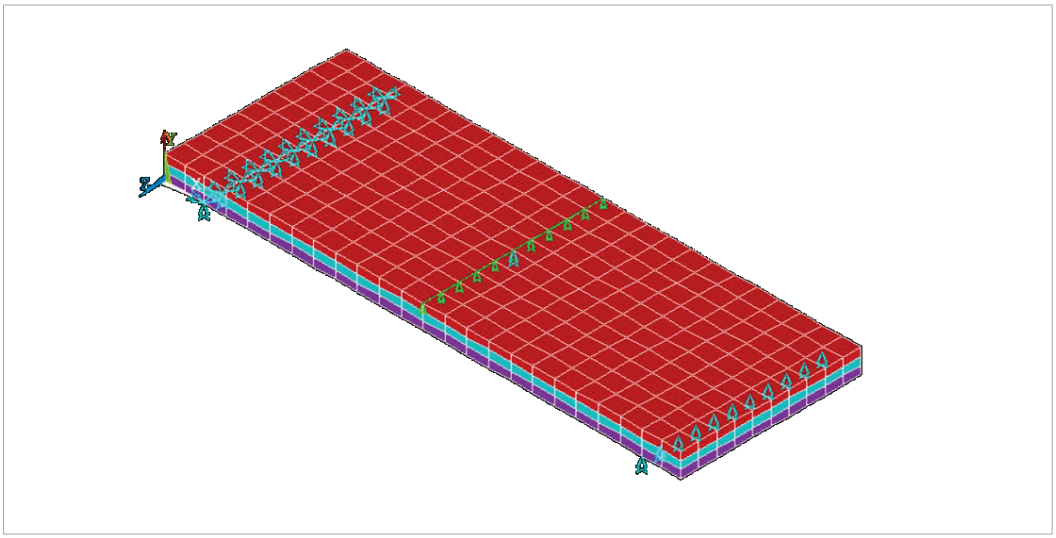


Fig. 3

Finite-element mesh and real constants (shown by colours) for Model 2.

	For slabs NAC-Steel; NAC-GFRP and RAC-GFRP1			For slab RAC-GFRP2		
	Direction	Rebars	Unit Volume Ratio	Direction	Rebars	Unit Volume Ratio
Bottom	X	5N10	0.01870	X	15N10	0.02020
	Y	12N6	0.00565	Y	12N6	0.00565
Top	X	5N4	0.00299	X	15N4	0.00898
	Y	12N4	0.00251	Y	12N4	0.00251

Table 4

ANSYS real constants for Model 2.

Using these two models, nonlinear analyses are performed for the four slabs shown in Fig. 1. The crack patterns, cracking loads, and maximum loads obtained from the models are compared with the experimental results.

Before comparison with the experimental data, several preliminary analyses are performed.

It is well known that the cracking process often causes convergence difficulties in numerical analyses using force-controlled loading. As a preliminary step, both loading approaches were tested for the two models. The results show that, after the main cracking process, the responses obtained with the two loading approaches are similar. This is because, after cracking, the reinforcement remains a load-bearing component and is modelled as a linear-elastic material. The main difference between the two loading approaches occurs during cracking. Under force-controlled loading, the cracking process is not captured sufficiently well, and the calculated cracking load is substantially lower than that obtained with displacement control. Therefore, displacement-controlled loading is used for the numerical analyses presented in the following section.

A preliminary mesh-sensitivity analysis was also performed. First, a linear static analysis was conducted and compared with a shell-element solution to determine the required number of elements, n, through the slab thickness. Four regular meshes were considered (Mesh 1, n = 1; Mesh

2, n = 2; Mesh 3, n = 3; and Mesh 4, n = 6). The mesh divisions in the other slab dimensions were adjusted proportionally. A load of 35,000 N was applied, and a linear-elastic material with E = 35,400 N/mm² was assumed. The slab deflections were compared. The difference between the shell-element solution and the four solid-element meshes ranged from 44% for Mesh 1 to 0% for Mesh 4; Mesh 3 differed by 3%. Thus, three elements through the slab thickness are sufficient to represent the bending shape of the slab. Using six elements through the thickness results in a very dense mesh in the other dimensions, which in turn causes convergence difficulties in the nonlinear analysis.

An in-plane mesh-sensitivity study was performed for the NAC-Steel slab using nonlinear analyses. Four meshes were considered. Two corresponded to Model 1 and Model 2, and two additional regular meshes, M1 and M2, were included. The total numbers of elements, N, were as follows: M1, N = 180; Model 1, N = 336; Model 2, N = 720; and M2, N = 2,880. The analyses were performed under displacement control with a maximum displacement of 16 mm. The cracking load, the corresponding displacement, and the force at the final step were compared. The difference in cracking load ranged from 11% between Model 1 and M1 to 3.2% between M2 and Model 2. The corresponding displacement differences ranged from 12.2% to 3.6%. At the final step, the results were practically identical. As expected, the percentage differences decreased with increasing mesh density. The absolute values of the cracking load and corresponding displacement also decreased. This occurs because increasing the number of elements reduces the overall numerical stiffness of the slab. Element displacements therefore increase, and the corresponding stress gradients cause the maximum tensile stress to be reached earlier at the Gauss points. This effect also leads to a denser crack pattern, as discussed in the following section. The results indicate that the mesh used in Model 2 is sufficiently refined for the subsequent analyses. The M2 mesh is very dense and causes convergence difficulties.

Results and Discussion

The experimental data for all slabs were obtained from Zaharieva et al. (2022) and Traykova et al. (2024).

Results for the NAC-Steel Slab

This slab is made of natural aggregate concrete and steel reinforcement. Material data are presented in Tables 1 and 2. The static scheme is shown in Fig. 1(c), and the reinforcement distribution is shown in Fig. 2(a). The deformed shapes at the final stage for both models are shown in Fig. 4. The crack patterns from the two models and the experimental crack distribution are shown in Fig. 5.

In ANSYS, concrete crushing at a Gauss point is indicated by an octagonal symbol, while crack formation is indicated by circles of different colours. Red marks the first crack, green the second, and blue the third. The crack pattern shown in Fig. 5 is displayed in transparent view and is practically the same on the bottom and top faces of the slabs.

The load-deflection curves for Model 1 and Model 2 are compared with the experimental data in Fig. 6(a). Key results are compared in Table 5.

Table 5
Results for the NAC-Steel slab.

	First crack		Maximum Load	
	Load [N]	Deflection [mm]	Load [N]	Deflection [mm]
Experiment	10 673	2.43	29 597	17
Model 1	10 027	0.69	34 490	16
Model 2	8 409	0.58	32 568	15

The results obtained with Model 1 and Model 2 are similar. Compared with the experiment, the numerical simulations predict lower cracking loads and corresponding deflections, while the maximum-load predictions and corresponding deflections also differ from the experimental values.

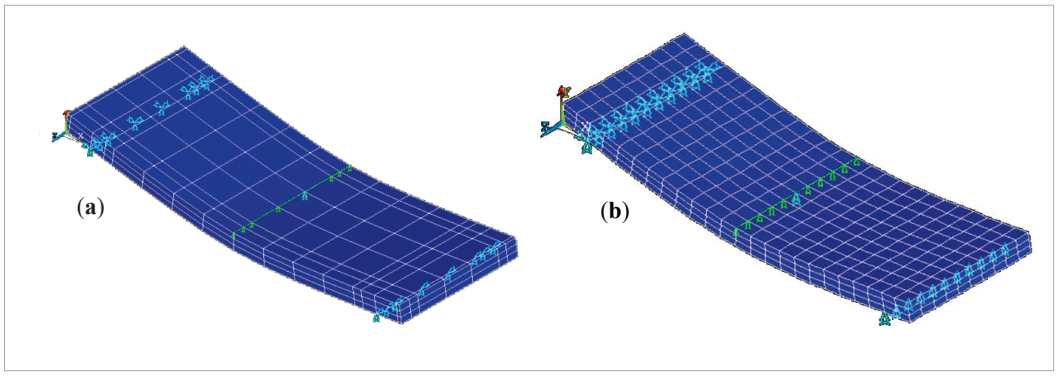


Fig. 4

Deformed shapes of the NAC-Steel slab:
a Model 1; **b** Model 2.

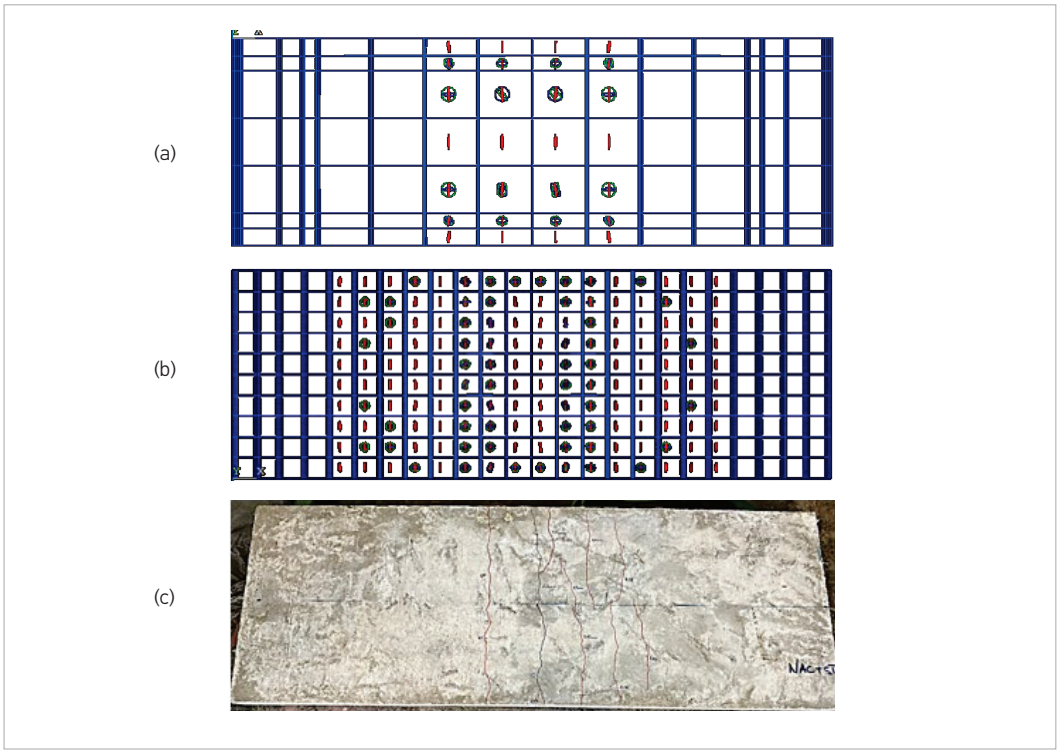


Fig. 5

Crack patterns of the NAC-Steel slab:
a Model 1;
b Model 2;
c experiment.

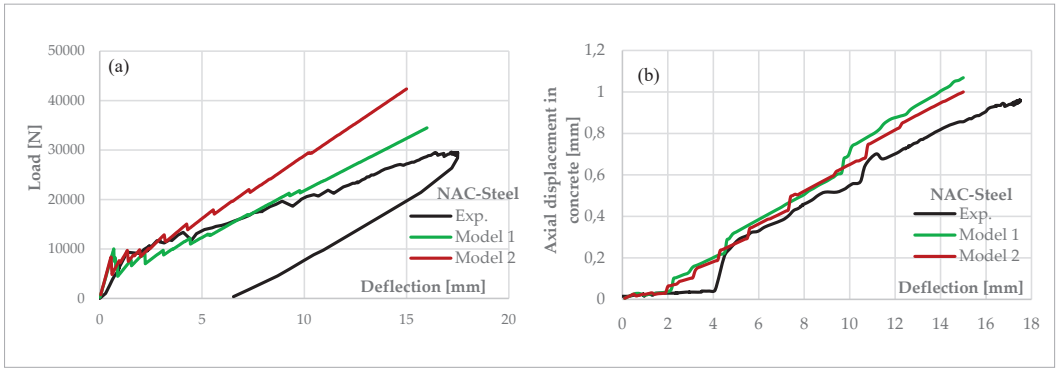


Fig. 6

a Load-deflection curves;
b axial displacement in concrete versus deflection for the NAC-Steel slab.

The numerical slabs are slightly stiffer. Model 1 agrees more closely with the experimental results than Model 2, which may be related to its smaller number of finite elements. Overall, the numerical results show good agreement with the experiment. However, as noted above, when the

reinforcement is modelled as elastic-plastic, yielding occurs in the rebars, contrary to the experimental observations. A possible explanation is the higher stiffness of the numerical models. Axial displacement is compared in Fig. 6(b) and is measured at point A (see Fig. 1(c)) along the slab length. The two numerical models give similar results and are close to the experimental data. The main difference occurs in the maximum displacement values. Because the numerical analyses use displacement-controlled loading, whereas the experiment is force-controlled, this difference is expected. Another difference is the jump in axial displacement associated with significant horizontal crack formation at a deflection of approximately 4 mm. The likely reason for this jump is the absence of dowel action in the numerical model. Nevertheless, the numerical solutions are sufficiently accurate for practical use.

Results for the NAC-GFRP Slab

For this slab, glass-fibre-reinforced polymer (GFRP) bars are used. GFRP is modelled as a linear-elastic material because the stresses in the structure do not exceed its tensile strength. Material data are presented in Tables 1 and 2. The slab static scheme is shown in Fig. 1(c), and the reinforcement distribution in Fig. 1(a). Crack patterns from Model 1, Model 2, and the experiment are shown in Fig. 7. The load-deflection curves are presented in Fig. 8(a), and key results in Table 6. Fig. 8(b) compares the reinforcement strain in a middle bar (point B in Fig. 1(a)).

Table 6
Results for the NAC-GFRP slab.

	First crack		Maximum Load	
	Load [N]	Deflection [mm]	Load [N]	Deflection [mm]
Experiment	11 782	1.41	29 508	41
Model 1	8 373	0.58	28 830	50
Model 2	8 636	0.6	33 509	50

For the NAC-GFRP slab, the numerical cracking loads are lower than the experimental value, while the maximum-load predictions differ between the two models; Model 1 is close to the experimental maximum load, whereas Model 2 overestimates it (Table 6). Model 2 gives a cracking load slightly closer to the experiment. Model 1 is softer than Model 2, which is unexpected because the smaller number of finite elements in Model 1 would normally suggest higher stiffness. This behaviour is mainly related to the reinforcement distribution. In Model 2, the reinforcement is uniformly distributed, which increases the model stiffness. This effect is more significant for weaker materials. Similar behaviour for the RAC-GFRP1 and RAC-GFRP2 slabs was reported by Traykova et al. (2024). The crack pattern from Model 1 agrees better with the experimental pattern because its reinforcement distribution more closely represents the actual reinforcement. The reinforcement strains from the two numerical models are practically identical. Because the cracking load in the numerical simulations is lower than in the experiment, the difference in the onset of softening is expected (Fig. 8(b)). Overall, the reinforcement strain increases at approximately the same rate as in the experiment.

Results for the RAC-GFRP1 Slab

For this slab, recycled aggregate concrete is used, with 30% of the coarse aggregate replaced by high-quality, industrially produced recycled aggregate. The combination of GFRP rebars and RAC is promising for practical applications, particularly in concrete structures exposed to aggressive environments. The purpose of this analysis is to assess whether the Willam-Warnke material model and SOLID 65 can be used to model different concrete and reinforcement materials, including RAC and GFRP. The physical characteristics of RAC are similar to those of natural aggregate concrete because the recycled aggregate is of high quality. The main difficulties in the present simulations are related to the brittle behaviour of GFRP and the sensitivity of the bond, especially in combination with RAC. In this study, the tensile-strength limit is not reached; therefore, brittle

rupture is not modelled. Material data are presented in **Tables 1** and **2**. The static scheme is shown in **Fig. 1(c)**, and the reinforcement distribution in **Fig. 1(a)**.

The numerical and experimental results are compared in **Fig. 9**, **Fig. 10**, and **Table 7**.

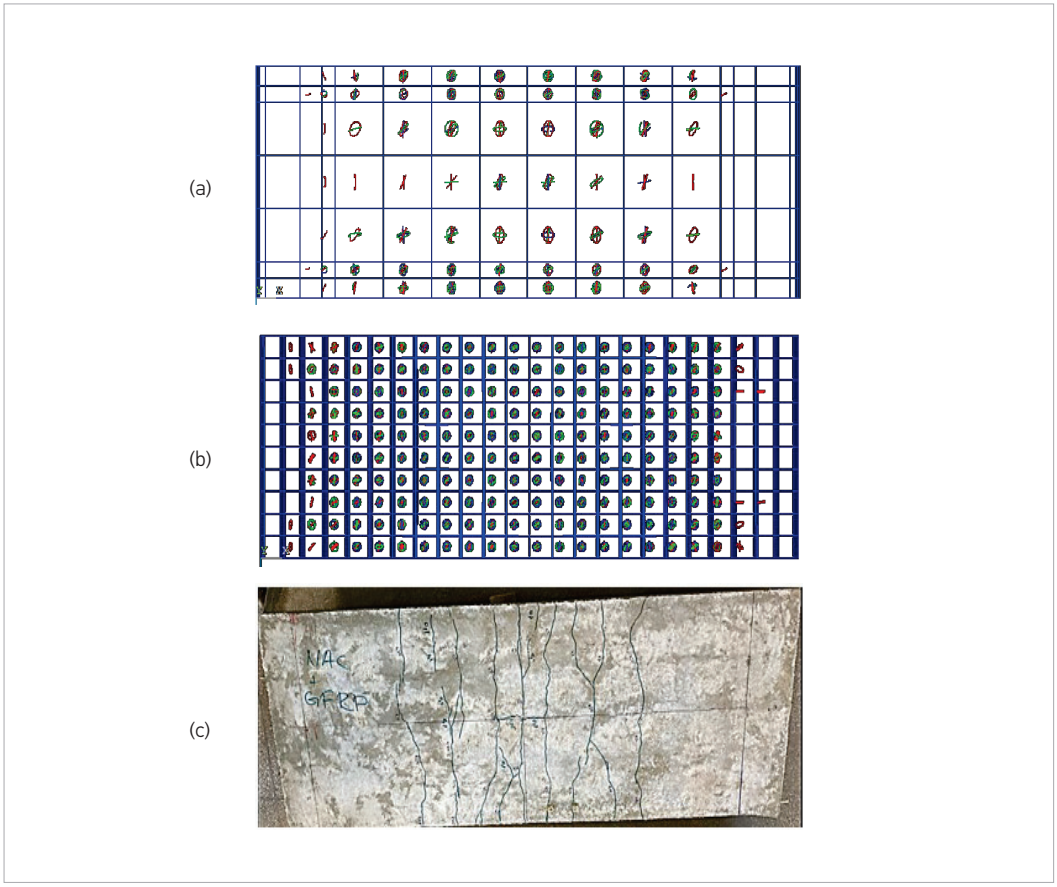


Fig. 7

Crack patterns of the NAC-GFRP slab:
a Model 1;
b Model 2;
c experiment.

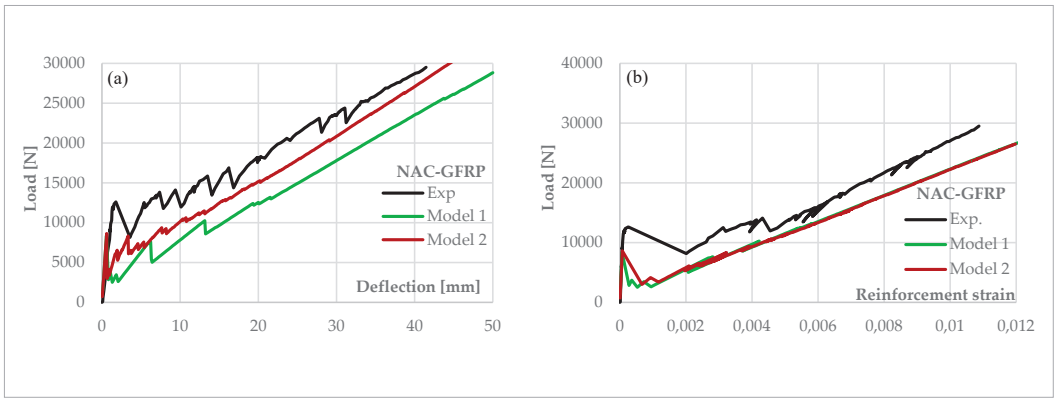


Fig. 8

a Load-deflection curves;
b load versus reinforcement strain for the NAC-GFRP slab.

	First crack		Maximum Load	
	Load [N]	Deflection [mm]	Load [N]	Deflection [mm]
Experiment	9 840	1.25	29 970	54
Model 1	9 101	0.58	30 535	50
Model 2	8 605	0.55	28 181	42

Table 7

Results for the RAC-GFRP1 slab.

Fig. 9

Crack patterns of the RAC-GFRP1 slab:
a Model 1;
b Model 2;
c experiment.

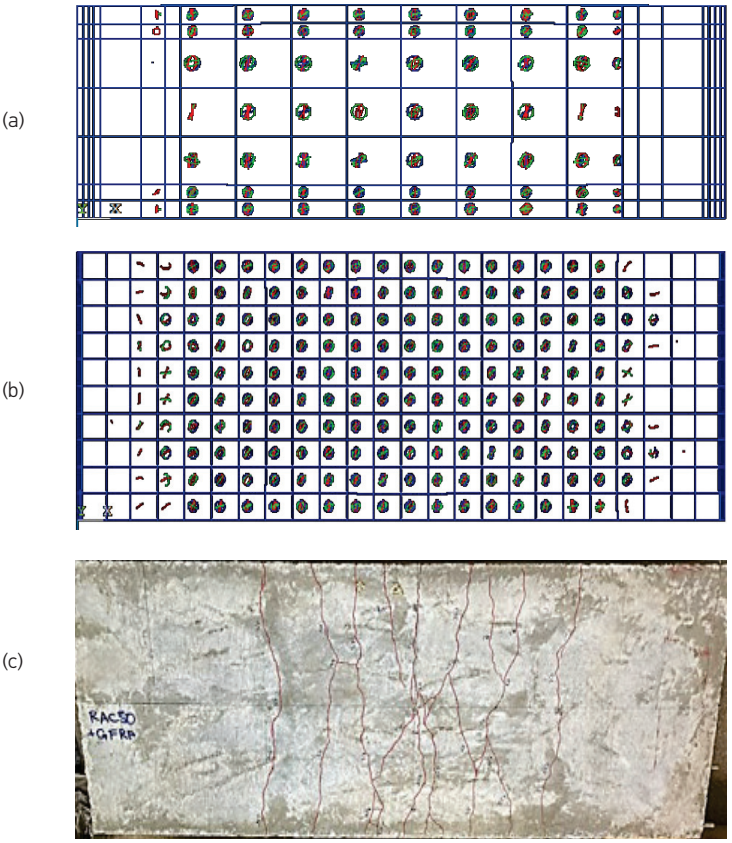
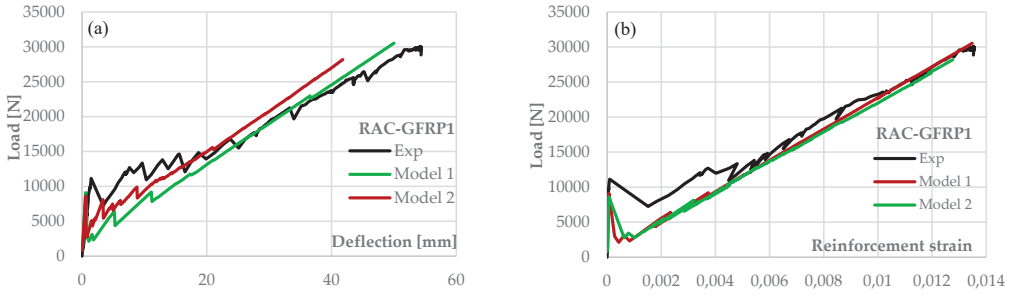


Fig. 10

a Load-deflection curves;
b load versus reinforcement strain for the RAC-GFRP1 slab.



The results in the figures and **Table 7** show that, in this case, the numerical simulations are closer to the experimental results than in the previous cases. This applies to deflection, cracking load, maximum load, and reinforcement strain. These results indicate that RAC combined with GFRP reinforcement can be modelled satisfactorily using the SOLID 65 finite element. In addition, Model 1 provides a better simulation of this slab's behaviour.

Results for the RAC-GFRP2 Slab

The final slab uses the same materials as the previous slab but a different reinforcement distribution, as shown in **Fig. 1(b)**. The purpose of this variation is to investigate the influence of reinforcement distribution on slab behaviour. Implementing Model 1 for this slab would require a very

dense mesh, comparable to that of Model 2, because the spacing between rebars is only 45 mm. Given the dense reinforcement arrangement, only Model 2 is used. The results are presented in Fig. 11, Fig. 12, and Table 8.

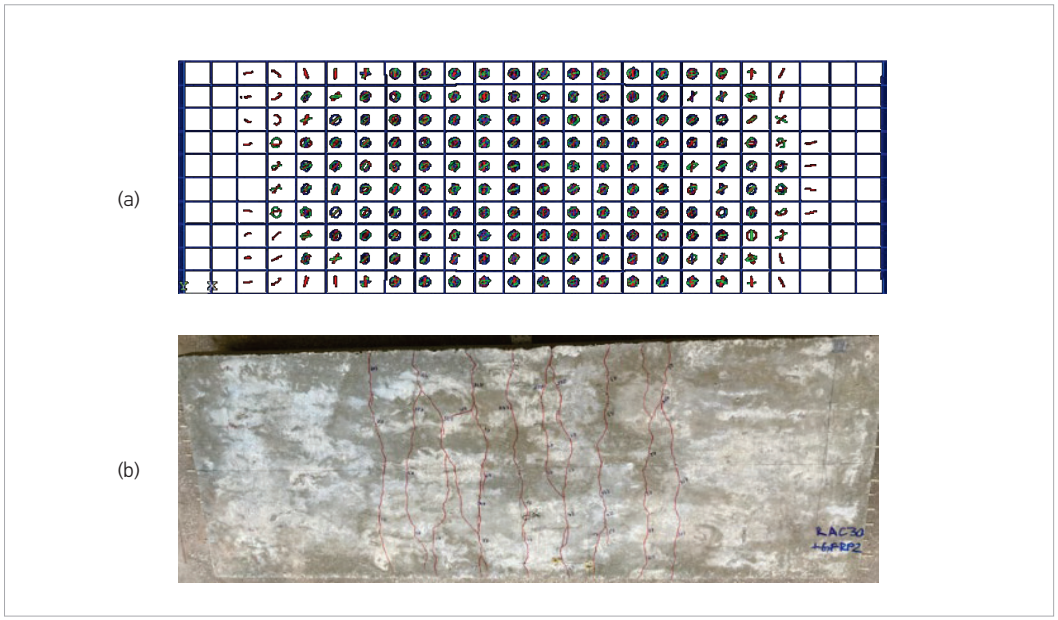


Fig. 11

Crack patterns of the RAC-GFRP2 slab:
a Model 2;
b experiment.

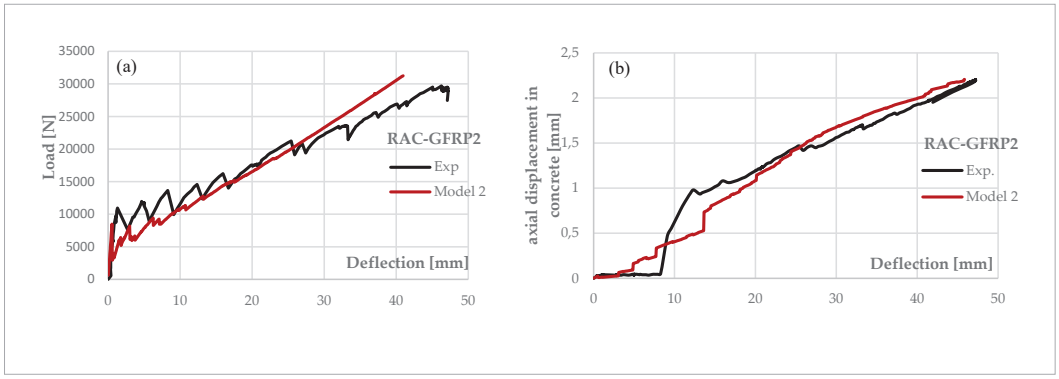


Fig. 12

a Load-deflection curves;
b axial displacement in concrete versus deflection for the RAC-GFRP2 slab.

	First crack		Maximum Load	
	Load [N]	Deflection [mm]	Load [N]	Deflection [mm]
Experiment	10 948	1.31	29 970	54
Model 2	8 480	0.54	31 244	41

Table 8

Results for the RAC-GFRP2 slab.

As expected, the numerical results for this slab agree more closely with the experimental results than the previous Model 2 results. This is because the slab has a dense reinforcement distribution that is better represented by Model 2. The numerical model predicts more cracks than observed in the physical experiment. According to Dere and Dede (2011), one possible explanation is that numerically predicted cracks correspond to clearly visible experimental cracks only when cracks are open in all three directions.

The axial displacement results are shown in Fig. 12(b) and agree very well with the experiment. The main difference is a jump in axial displacement associated with significant horizontal crack

formation at a deflection of approximately 9 mm. Nevertheless, the numerical solution shows very good agreement for practical purposes.

Fig. 10(a) and Fig. 12(a) show that the RAC-GFRP2 slab has a smaller deflection than RAC-GFRP1 at a similar maximum load. This suggests that denser reinforcement distribution reduces slab flexibility (i.e., increases stiffness), as expected. Further details are provided by Zaharieva et al. (2022) and Traykova et al. (2024).

Summary of Results

Tables 5-8 show that, in all cases, the cracking load and corresponding displacement predicted by the numerical simulations are lower than the experimental values. At the final stage, the numerical results are close to the experimental results.

The largest difference between the two models is 16% for the cracking load and corresponding displacement of the NAC-Steel slab. In the other cases, the difference is less than 5%. The largest difference between numerical modelling and the experiment is 26% for the cracking load and corresponding displacement of the NAC-GFRP slab. In the remaining cases, the cracking load predicted by Model 1 is closer to the experimental value than that predicted by Model 2.

Comparison of Fig. 6(a) and Fig. 12(a) illustrates the difference in dowel action between GFRP and steel reinforcement. The experimental curves indicate significantly lower adhesion between concrete and GFRP reinforcement.

Conclusions

During numerical modelling, several significant difficulties and limitations were identified:

- The shear stiffness of the reinforcing bars cannot be modelled; consequently, dowel action is excluded from the shear-transfer mechanism.
- Yielding appears in the steel reinforcement in the numerical model, contrary to the experimental results. To remain consistent with the experimental observations, the steel was therefore modelled as linear elastic.
- Modelling GFRP reinforcement as a purely brittle material is difficult in practice. The tensile strength of GFRP is sufficiently high that rupture was not observed in the experiments. Therefore, GFRP was modelled as a linear-elastic material.
- The theoretical model for concrete (NAC and RAC30) was adopted using the default software settings because sufficient material data were not available.
- For the shear-retention factors, values between 0.5 and 0.6 for β1 and 1.0 for β2 are recommended.
- Force-controlled loading does not capture the cracking process adequately. Therefore, displacement-controlled loading is recommended. Despite these modelling limitations, the numerical simulations show good agreement with the experimental results.
- From a practical perspective, the following conclusions can be drawn regarding the two modelling approaches (discrete - Model 1 and smeared - Model 2):
- Both models predict lower cracking loads and corresponding displacements than observed experimentally. Model 1 generally provides closer agreement than Model 2.
- The numerical crack patterns are more extensive than those observed experimentally but still provide a clear representation of crack distribution.
- The crack distribution predicted by Model 1 is closer to the experimental results than that predicted by Model 2.
- For densely distributed reinforcement, Model 1 would practically coincide with Model 2 and therefore offers little additional benefit.

- Additional experimental comparisons are needed to improve and further validate both models.

The main differences between the numerical models and the experiment occur during crack formation. The numerical models predict a smoother cracking process than observed experimentally. This may be related to the use of displacement-controlled loading in the numerical analyses versus force-controlled loading in the experiment. Another contributing factor may be the absence of dowel action in the numerical model.

With respect to the use of RAC and GFRP in structural design and their sustainability implications, the following conclusions can be drawn:

- Recycled aggregate concrete (RAC) reinforced with GFRP rebars can be successfully modelled using the SOLID 65 finite element in ANSYS, subject to the limitation that dowel action is not represented.
- Conventional theoretical models can be applied to the flexural behaviour of GFRP-reinforced RAC and can subsequently be used for dimensioning structural elements such as slabs.
- The larger deflections of GFRP-reinforced slabs can be reduced to some extent by decreasing the spacing between GFRP rebars.
- Combining RAC with GFRP reinforcement can help address some durability issues.
- Given the importance of recycled materials for sustainability, numerical modelling of RAC and GFRP can support their wider application in sustainable construction.

Acknowledgment

The numerical part of this study was supported by the project "MOBile and Innovative Circularity for CONstruction PROducts (MOBICCON-PRO)", co-funded by the European Union's Horizon Europe programme under Grant Agreement No. 101091679.

Funding

The experimental part of this research was funded by Project BG05M2OP001-1.002-0019, "Clean Technologies for Sustainable Environment - Water, Waste, Energy for Circular Economy", financed by the Operational Programme "Science and Education for Smart Growth" 2014-2020 and co-financed by the European Union through the European Structural and Investment Funds.

Use of Artificial Intelligence Tools

During the preparation of this article, the author used Google Translate to support language editing and improve text clarity. The author independently reviewed and revised the content and assumes full responsibility for the accuracy and integrity of the work.

References

Al-Maliki, H. N. G., Alshimmeri, A. J. H., Al-Balhawi, A., & Zhang, B. (2023). Numerical simulations on the flexural behaviours of reinforced concrete girders strengthened with bolts. Buildings, 13, 1044. https://doi.org/10.3390/buildings13041044

ANSYS, Inc. (2024). Ansys Academic Research Mechanical, Release 2024 R1, Help System: Coupled Field Analysis Guide.

Assad, M., Hawileh, R., & Abdalla, J. (2022). Finite element simulation of FRP-strengthened thin RC slabs. Journal of Composites Science, 6, 263. https://doi.org/10.3390/jcs6090263

Avci, O., & Bhargava, A. (2019). Finite-element analysis of cantilever slab deflections with ANSYS SOLID65 3D reinforced-concrete element with cracking and crushing capabilities. Practice Periodical on Structural Design and Construction, 24, 05018007. https://doi.org/10.1061/(ASCE)SC.1943-5576.0000411

Bondok, M. H., Debaiky, A. S., & Makhlouf, M. H. (2023). Numerical investigations of GFRC beams

strengthened in shear with innovative techniques. Mansoura Engineering Journal, 48(2). https://doi.org/10.58491/2735-4202.3023

CEB-FIP. (1993). CEB-FIP Model Code 1990: Design code (Bulletin d'Information Nos. 213/214).

Dahmani, L., Kaci, S., & Khennane, A. (2010). Crack identification in reinforced concrete beams using ANSYS software. Strength of Materials, 42, 232-240. https://doi.org/10.1007/s11223-010-9212-6

Dere, Y., & Dede, F. T. (2011). Nonlinear finite element analysis of an R/C frame under lateral loading. Mathematical and Computational Applications, 16, 947-958. https://doi.org/10.3390/mca16040947 Emarah, D. A. (2019). Numerical study to investigate the behavior of reinforced concrete slabs with CFRP sheets. Water Science, 33, 142-153. https://doi.org/10.1080/11104929.2019.1688068

Gherbi, A., Dahmani, L., & Boudjemia, A. (2018). Study on two-way reinforced concrete slab using ANSYS with different boundary conditions and loading. International Journal of Civil and Environmental Engineering, 12, 1151-1156. https://www.researchgate.net/publication/329372034

Jebur, H. S. (2021). Nonlinear finite element analysis of reinforced and plain concrete haunched beams under torsion. Civil and Environmental Engineering, 17, 229-241. https://doi.org/10.2478/cee-2021-0024

Kaya, N., & Anil, Ö. (2021). Prediction of load capacity of one-way reinforced concrete slabs with openings using nonlinear finite element analysis. Journal of Building Engineering, 44, 102945.

https://doi.org/10.1016/j.jobe.2021.102945

Mahmoud, A. A., El Gani, B. K., Mustafa, T. S., & Khater, A. N. (2024). Experimental, numerical, and analytical investigation of the reinforced concrete hidden and wide beams. International Journal of Concrete Structures and Materials, 18, 73. https://doi.org/10.1186/s40069-024-00709-5

Manjunath, H. R., & Prabhakara, R. (2019). Analysis of flexural behavior of doubly reinforced high-strength concrete beams using ANSYS. IJSR International Journal of Science and Research, 8, 392-396. https://www.ijsr.net/archive/v8i1/ART20194190.pdf

Musmar, M. A., Rjoub, M. I., & Abdel Hadi, M. A. (2014). Nonlinear finite element analysis of shallow reinforced beam using Solid 65 element. ARPN Journal of Engineering and Applied Sciences, 9, 85-89. https://arpnjournals.com/jeas/research_papers/rp_2014/jeas_0214_1003.pdf

Pacheco, J., de Brito, J., & Lamperti, T. M. (2023). Use of recycled aggregates in concrete: Opportunities for upscaling in Europe. Publications Office of the European Union. https://doi.org/10.2760/144802

Parvanova, S., Kazakov, K., Kerelezova, I., Gospodinov, G., & Nielsen, M. P. (2005). Modelling the nonlinear behavior of R/C beams with moderate shear span and without stirrups using ANSYS. In Proceedings of International Conference VSU 2005 (pp. 65-70). VSU.

RILEM. (1996). Technical recommendations for testing and use of construction materials: RC6, Bond test for reinforcing steel: 2. Pull-out test. https://doi.org/10.1617/2351580117.081

Smarzewski, P., & Słowik, M. (2023). Numerical analysis of cracking processes in RC beams without transverse reinforcement. Processes, 11, 584. https://doi.org/10.3390/pr11020584

Tabish, F., Raza, A., Ullah, S., & Jameel, M. S. (2022). Investigation of flexural behavior of reinforced concrete beams using 3D finite element analysis. Numerical Methods in Civil Engineering, 7, 37-56. https://doi.org/10.61186/nmce.2022.343

Tjtradi, D., Eliatun, E., & Taufik, S. (2017). 3D ANSYS numerical modeling of reinforced concrete beam behavior under different collapsed mechanisms. International Journal of Mechanics and Applications, 7, 14-23. https://doi.org/10.5923/j.mechanics.20170701.02

Tran, D.-B., & Cajka, R. (2022). The ultimate load of the fiber-reinforced concrete slab foundations subjected to the concentrated load by ANSYS. International Research Journal of Multidisciplinary Technovation, 4, 18-26. https://doi.org/10.54392/irjmt2253 https://doi.org/10.54392/irjmt2253

Traykova, M., Zaharieva, R., & Kerelezova, I. (2024). Potential in the structural application of GFRP bars reinforcement as an alternative for recycled aggregate concrete slab. In Construction's Role for a World in Emergency: Proceedings of IABSE Symposium Manchester 2024 (pp. 1051-1057). IABSE. https://doi.org/10.2749/manchester.2024.1051

Vintimilla, C., & Etxeberria, M. (2023). Limiting the maximum fine and coarse recycled aggregates-Type A used in structural concrete. Construction and Building Materials, 380, 131273. https://doi.org/10.1016/j.conbuildmat.2023.131273

Zaharieva, R. A., Traykova, M. D., & Dimitrov, G. A. (2022). Challenges in the structural application of recycled aggregate concrete reinforced with GFRP rebars - Part 1: Structural aspects. In Proceedings of the 6th fib International Congress 2022 (pp. 162-170).

About the authors

IRINA KERELEZOVA

Associate Professor

PhD, Department of Structural Mechanics, Faculty of Civil Engineering, University of Architecture, Civil Engineering and Geodesy, Sofia, Bulgaria

Main research area

Fracture mechanics; finite element modelling

Address

1 Hr. Smirnenski Blvd., Sofia 1046, Bulgaria
E-mail: igk_fce@uacg.bg

This article is an Open Access article distributed under the terms and conditions of the Creative Commons Attribution 4.0 (CC BY 4.0) License (http://creativecommons.org/licenses/by/4.0/).